MDPI

Article

On the symmetry of the bone density over the nasopalalatin foramen via a mathematical fractal dimension analysis

Michael M. Bornstein[1], Manuel Fernández-Martínez [2], Juan L.G. Guirao [3,]0000-0003-2788-809X, Francisco J. Gómez-García[4], Yolanda Guerrero-Sánchez[4] and Pía López-Jornet[4]

[1] Department of Applied Oral Sciences of the Faculty of Dentistry, University of Hong Kong; bornst@hku.hk
[2] University Centre of Defence at the Spanish Air Force Academy, MDE-UPCT, 30720 Santiago de la Ribera, Murcia, SPAIN; manuel.fernandez-martinez@cud.upct.es
[3] Departamento de Matemática Aplicada y Estadística. Universidad Politécnica de Cartagena, Hospital de Marina, 30203-Cartagena, Región de Murcia, Spain; juan.garcia@upct.es
[4] Department of Dermatology, Stomatology, Radiology and Physical Medicine, Morales Meseguer General Universitary Hospital, Avda. Marqués de los Vélez, 30008 Murcia, Spain; fjgomez@um.es, yolanda.guerreros@um.es, majornet@um.es.
* Correspondence: juan.garcia@upct.es; Tel.: +34-968-338913
† These authors contributed equally to this work.

Version December 18, 2018 submitted to Journal Not Specified

Abstract:
The objective of the present paper is to describe all the anatomical considerations that surround the nasopalalatin foramen, relating them to the study of bone density, through the fractal dimension, in that same area. We consecutively selected a sample of 100 patients all of them with CBCTs (cone beam computed tomography) performed for treatment needs. We chose a specific window (ROI), which coincides with an axial cut at the level of the anterior nasal spine. We shall analyze different anthropometric measurements together with a novel analysis of the fractal dimension. In turn, our initial sample was subdivided into three groups: group 1 (without loss of teeth), group 2 (absence of some teeth), and group 3 (total edentulous). We applied both Mann-Whitney test and Student's t-test to obtain the statistical results. The sample consisted of a total of 77 patients, of which 63 are women (81.8% of the total). A total of 60 subjects were assigned to group 1, 10 to group 2, and 7 to group 3. The mean age of the patients in that sample was 53.2 years with a standard deviation of 9 years. We conclude, that the mathematical invariant *fractal dimension* behaves symmetrically for binary images from the scanner of each subject of our study sample. We also conclude that there were no significant differences between all the anthropometric measures used neither in the subjects themselves nor in the different groups. Therefore, a pattern of symmetry was appreciated at all levels.

Keywords: Fractal dimension; nasoplatine foramen; cone beam computed tomography.

1. Introduction

Embryologically, the formation (histogenesis) and mineralization (ossification) of the hard facial tissues takes place after that of the soft tissues, at the end of the embryonic period ($10-12$ weeks). There are two types of ossification, on the one hand intramembranous, which is made from the mesenchyme, which will become osteoid ossification centers, and will be arranged forming a three-dimensional network of trabeculae; the other type is the endochondral or cartilaginous mold, in which a cast of hyaline cartilage will be replaced by bone tissue. That there is one type or another is intimately related to the future function of the bone. In areas of growth exposed to stress, the mechanism of ossification

is intramembranous. Where there is pressure is, the ossification is endochondral, since the cartilage is rigid and flexible, supporting this type of loads very well. In the bones of the face or viscerocranium, intramembranous ossification predominates. The maxillary bone begins its ossification at the end of the sixth week of intrauterine life, and takes place from two points, one in the anterior (premaxillary) and another in the posterior (postmaxillary) area. The trabeculae formed from the premaxillary ossification center are rapidly directed in 3 directions: 1) upward to form the anterior wall of the descending process; 2) forward toward the anterior nasal spine and 3) downward to form the alveolar processes of the upper incisors. Cranial and facial growth is performed in the three dimensions of space. Normally it is harmonic and proportional, but not uniform. This growth is produced by the combination of four different biological phenomena: 1) Replacement of cartilage by bone; 2) Growth at suture level; 3) Peripheral bone affectation associated with internal resorption and 4) Dental rash [5]. Anatomically, the maxillary bone is part of the mass or facial bone complex, being the functional center of it. The external configuration of the upper jaw is very irregular. However, you can recognize a quadrilateral shape and distinguish two faces, one external and one internal, and four edges. The maxillary bone is even and fused in the midline by the intermaxillary suture and constitutes the center of the upper facial mass, forming part of the buccal cavity, the bony palate, the orbital, nasal, pterygopalatine and zygomatic pits. The maxillary bone consists of

- Body, is most of the bone, pyramidal, part of the orbit, nasal cavity, infratemporal fossa and middle third of the face. In its anterior region it presents the anterior nasal spine and the nasal notch.
- Frontal apophysis, which articulates with the nasal, frontal, ethmoid and lacrimal bones.
- Zygomatic apophysis that articulates medially with the maxillary process of the zygomatic bone.
- Palatine process, extending medially forming the greater part of the hard palate, articulating in the middle line with that of the contralateral maxilla and later with the palatal bone.
- Alveolar process, which supports the upper teeth. The convex region that covers the canine by vestibular is the canine eminence, mesial to this there is a concavity, the incisive fossa, and distal to the canine there is another concavity, the canine fossa. The most posterior region of the alveolar process is the tuberosity of the maxilla [15].

Topographically, there are three zones:

1. Anterior zone: From the intermaxillary suture to the canine eminence,
2. Middle zone: Canine eminence and the zygomatic-alveolar or infratemporal crest, and
3. Posterior zone: Distal to the zygomatic-alveolar crest.

The anterior maxilla, also called the premaxilla area, contains an important anatomical structure, the anterior palatal, incisor or nasoplatine (NC) canal. The CN is located immediately below the incisive papilla. Both anterior palatine ducts open into the incisive fossa of the osseous palate and possibly pass through the junction line of the incisor (premaxillary) bone with the maxilla. It is the primitive communication between the mouth and the nose. The CN was first described in a general way by Stenson in 1683. It is located in the midline of the palate, posterior to the central incisors and below the interincisal papilla. It is projected vertically in the premaxillary region and consists of two extremes: one towards the nasal floor with two openings that are directed towards each side of the septum, known as foramines or Stenson holes; the second end corresponds to the opening towards the oral cavity, called incisor hole whose diameter is 3.62 mm. This anatomical structure houses the nasoplatine nerve and the nasoplatine artery, which originates from the sphenopalatine artery (terminal branch of the internal maxillary), both going to innervate and simultaneously irrigate the nasal floor mucosa and the anterior palatal mucosa. CN is also composed of fibrous connective tissue, fatty tissue and some minor salivary glands [9]. The balance, symmetry and harmony between the facial structures are fundamental elements in the attainment of facial beauty the context in which the body and facial image, since it plays a fundamental role in the psychosocial development of the individual. In this sense, due to the close relationship of the teeth with the formation and preservation of alveolar processes,

the loss of these causes an irreversible process of reduction of bone volume, both horizontally and vertically, which is greater in the maxilla higher than in the jaw and vestibular than in the palatine, with serious clinical, functional and aesthetic implications [11]. The rhythm of this bone loss depends on several factors, such as the existence of more teeth in the arch, maneuvers performed for exodontia, the presence of previous infectious or cystic pathology, as well as the complication of healing by alveolitis. Patients with a long period of partial or total edentulism suffer severe atrophy of the jaws, with great asymmetry of the dental arches. As a consequence, the retention and stability of partial or complete removable prostheses is negatively affected [2]. Currently, in developed countries, dental implants are considered the best option to replace lost teeth with others (removable prosthesis or bridge). However, in case of bone deficiency the placement of the implants can be very complicated, especially in the maxilla, where the bone loss can be so pronounced that the floor of the maxillary sinus is practically in contact with the palatal fibromucosa. In these cases, it is necessary to perform maneuvers of bone volume increase to allow the placement of implants with greater length and diameter and in a more favorable position, thus improving the results in the medium and long term [10]. These advanced oral surgery techniques require a thorough morphological study of the area to be treated, for which 3D radiology is essential. When no distortion is found, this type of technique allows better planning of the implant treatment according to the receptor site. In this sense, the Cone Beam Computed Tomography (CBCT) allows the clinician to do a variety of analyzes to know the characteristics of bone structures, such as bone quality, or to inspect the topography and thickness of cortical bones. Bone volume can be examined essentially to predict vascularity for bone maturation and preservation. Bone defects can be detected that are crucial to decide on a graft procedure. The use of CBCT specialized in dentomaxillofacial area has been a step forward compared to conventional CT for its greater precision, lower cost, radiation, accessibility and short duration of the scanner [12]. The most relevant anatomical formation of the anterior region of the maxilla is the CN. In the scientific literature, surgical difficulties and anatomical limitations during implant surgery have been described in relation to the location of this structure. In the study conducted by Bornstein et al. [1] to evaluate the different anatomical variations of CN, we found a single channel that was identified in 45 cases, two parallel channels separated in 15 cases and variations of the "Y" type were observed in 40 cases. The dimensions of the CN revealed an average diameter of the nasal openings of 3.49 mm, and a broad incisive foramen with a diameter of 4.45 mm, the average length of the CN was 10.99 mm, the dimensions of the buccal bone plate showed an increasing width from the crest to the apical measurements. Liang et al. [8] in 2009, conducted a study to determine the anatomical variability of CN and determine its characteristics, both anatomical and histological. The diameter of the canal was found enlarged with age and in edentulous patients. In 2018, Hakbilen et al [6], analyzed three-dimensionally (CBCT) the anatomical dimensions of CN of 619 individuals aged $17 - 86$ years and correlated them with age, gender and edentulism status. They found large morphological differences between individuals. 26.17% had a conical shape, 24.71% hourglass, 16.80% were cylindrical, 15.83% funnel, 11.14% banana, and 5.33% of the channels were branched. Men and women showed significant differences in the length of the channels, as well as in the thickness of the vestibular cortices in the sagittal sections. Age and edentulism also affected the length of the CN and the thickness of the vestibular cortex.

The knowledge about the establishment of the theories that can clarify the etiopathogenesis of the development of the nasoplatine region and CN in humans is necessary for the understanding of the morphology of this region and the morbidity that takes place in it, being the tomography a great help for this purpose. Linked to all these types of studies that have been conducted there has never been a parallel study of the bone density analysis. The studies that we have reviewed always use the same technique to analyze this value, it is the box-counting technique ([1],[8]). As we have already explained in previous publications ([6],[13]), the method for us of choice is a much more precise algorithm that provides reliable results that are very close to reality. In summary, the objective of this work is to carry out an exhaustive analysis of the area surrounding the nasoplatine foramen, helping us with new mathematical techniques with the idea of finding a symmetry pattern that demonstrates that the bony

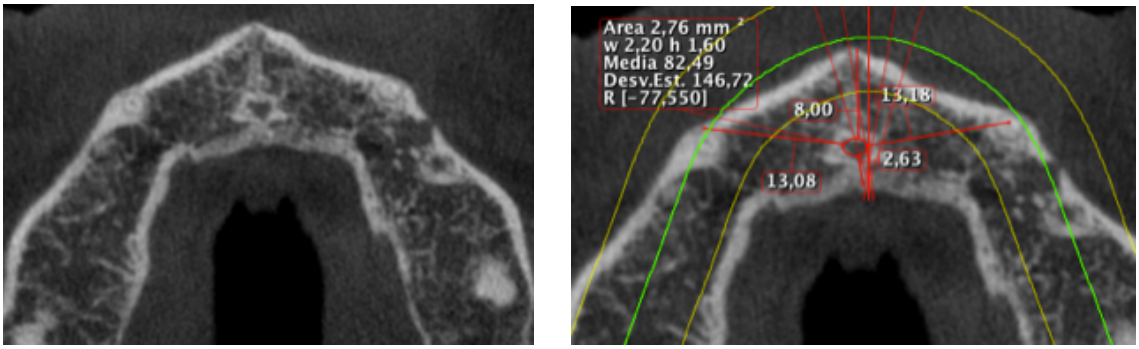

Figure 1. Cutting selection to be studied and taking measurements.

trabeculate resembles in its architecture a fractal and therefore has a fractal dimension that approaches real values.

2. Materials and Methods

This is a cross-sectional and observational clinical study where we selected a sample of 100 patients consecutively from the University dental clinic of Murcia (Spain). The study was approved by the Bioethics Committee of the University of Murcia. All individuals gave their informed consent in writing before participating. The inclusion criteria were applied: patients in health conditions both systemic and dental, not pregnant, images that do not contain artifacts. Of these 100 initial patients we had 77 that met all the criteria described above (5 were discarded because they were submitted to treatment with bisphosphonates and 18 since the images presented artefacts or were not considered with enough quality to be able to apply the algorithm). All CBCTs were performed using the same Planmeca® equipment, Planmeca ProMax 3-D Max (Planmeca Oy, Helsinki, Finland) calibrated according to technical considerations. X-rays were obtained with the patient in the same position (prone position). The beam emission parameters were kV $= 96$, mA $= 8$, exposure time of 12 seconds (11.94s) with an image size of $501 \times 501 \times 466$ voxels (each voxel being equivalent to 200 μm) The evaluation software used was the Romexis 2.5.1® program (Planmeca Oy, Helsinki, Finland), which allowed observing the image in a multiple window where the axial, coronal and sagittal planes can be visualized in 0.2mm intervals, in addition to a 3D vision. As indicated above, the sample was divided into three groups. We proceed to select a specific ROI that was obtained in the axial plane at the height of the nasal spine, visualising the nasoplatine foramen and the canine mamelons on both sides.

We proceed to make the following measurements: distance anterior wall nasoplatine hole to anterior nasal spine (DCV), distance back wall foramen (NF) to border palate bone (DCP), distance right side wall NF to right canine mamelon (DVD), distance left lateral wall NF to left canine mamelon (DVI), area of the NF and other series of values provided by the software itself: W, H, Mean, and standard deviation. All measurements were made by a single examiner duly trained for the purpose. The measurements were repeated by the examiner one month after performing the first ones and if there was a discrepancy in any measurement, the average of both is obtained and the kappa index was used. Once all the results were obtained, a database was created, and the necessary Mathematica® code was written to perform all the statistical analyses.

2.1. A novel approach for fractal dimension calculations

Let $\delta > 0$. A (plane) $\delta-$cube is a set of the form $[\delta\, k_1, \delta\,(1+k_1)] \times [\delta\, k_2, \delta\,(1+k_2)]$, where $k_1, k_2 \in \mathbb{Z}$. The standard definition of box dimension (for plane subsets) is provided below.

Definition 1. *Let $F \subseteq \mathbb{R}^2$. Its (lower/upper) box dimension is given by*

$$\underline{\dim}_{\mathrm{B}}(F) = \underline{\lim}_{\delta \to 0} \frac{\log \mathcal{N}_\delta(F)}{-\log \delta}.$$

$$\overline{\dim}_{\mathrm{B}}(F) = \overline{\lim}_{\delta \to 0} \frac{\log \mathcal{N}_\delta(F)}{-\log \delta}.$$

In particular, the box dimension of F, $\dim_{\mathrm{B}}(F)$, is defined through the following limit (if it exists):

$$\dim_{\mathrm{B}}(F) = \lim_{\delta \to 0} \frac{\log \mathcal{N}_\delta(F)}{-\log \delta},$$

where $\mathcal{N}_\delta(F)$ can be calculated as the number of $\delta-$cubes that intersect F.

The utility of box dimension lies in the fact that it can be easily calculated in empirical applications (mainly on Euclidean spaces) involving fractal dimension. In fact, it can be estimated as the slope of a regression line to compare $\log \delta$ vs. $\log \mathcal{N}_\delta(F)$ over a discrete collection of scales properly chosen.

Another key concept to tackle with fractal dimension calculation is fractal structure. First, we recall that a covering of a set X is a collection of subsets, Γ, such that $X = \cup\{A : A \in \Gamma\}$.

Definition 2. *Let $\mathbf{\Gamma} = \{\Gamma_n : n \in \mathbb{N}\}$ be a countable family of coverings of a given set X. We shall understand that $\mathbf{\Gamma}$ is a fractal structure provided that the two following statements hold:*

(i) for each $A \in \Gamma_{n+1}$, there exists $B \in \Gamma_n$ such that $A \subseteq B$.
(ii) $B = \cup\{A \in \Gamma_{n+1} : A \subseteq B\}$ for all $B \in \Gamma_n$.

It is worth mentioning that covering Γ_n of $\mathbf{\Gamma}$ is called as *level* n of that fractal structure. Equivalently, Definition 2 states that level $n+1$ is a strong refinement of level n of $\mathbf{\Gamma}$. Additionally, the levels of the natural fractal structure on $\mathbb{R}^2$, $\mathbf{\Delta} = \{\Delta_n : n \in \mathbb{N}\}$, are defined as

$$\Delta_n = \left\{ \left[\tfrac{k_1}{2^n}, \tfrac{1+k_1}{2^n}\right] \times \left[\tfrac{k_2}{2^n}, \tfrac{1+k_2}{2^n}\right] : k_1, k_2 \in \mathbb{Z} \right\}.$$

In particular, the natural fractal structure on $\mathbb{R}^2$ can be induced on the unit square by defining

$$\Delta_n = \left\{ \left[\tfrac{k_1}{2^n}, \tfrac{1+k_1}{2^n}\right] \times \left[\tfrac{k_2}{2^n}, \tfrac{1+k_2}{2^n}\right] : k_1, k_2 = 0, 1, \ldots, 2^n - 1 \right\}$$

The first two levels of the natural fractal structure on $[0,1] \times [0,1]$ are depicted in Fig. 2.

In this paper, we shall apply the following result to efficiently calculate the box dimension of a binary images from the CBCT scanner of each patient. Observe that it suffices with calculating the number of $\delta-$cubes that intersect $\alpha^{-1}(F) \subseteq [0,1]$ for (lower/upper) $\dim_{\mathrm{B}}(F)$ calculation purposes.

Theorem 1 (c.f. Corollary 2.6 in [4])**.** *Let $\mathbf{\Delta}$ be the natural fractal structure on $[0,1] \times [0,1]$ and assume that $[0,1]$ is endowed with the fractal structure $\mathbf{\Gamma}$ with levels given by $\Gamma_n = \{[\frac{k}{2^{2n}}, \frac{1+k}{2^{2n}}] : k = 0, 1, \ldots, 2^{2n} - 1\}$. In addition, let F be a subset of $[0,1] \times [0,1]$ and $\alpha : [0,1] \to [0,1] \times [0,1]$ a function with $\mathbf{\Delta} = \alpha(\mathbf{\Gamma})$. The (lower/upper) box dimension of F can be calculated by the following expressions:*

$$\underline{\dim}_{\mathrm{B}}(F) = 2 \cdot \underline{\lim}_{\delta \to 0} \frac{\log \mathcal{N}_\delta(\alpha^{-1}(F))}{-\log \delta}.$$

$$\overline{\dim}_{\mathrm{B}}(F) = 2 \cdot \overline{\lim}_{\delta \to 0} \frac{\log \mathcal{N}_\delta(\alpha^{-1}(F))}{-\log \delta}.$$

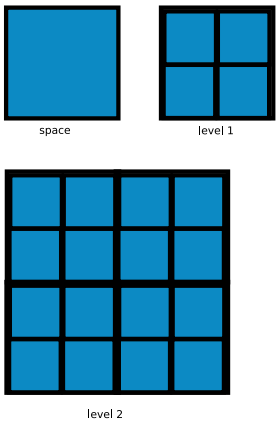

Figure 2. First two levels of the natural fractal structure on $[0,1] \times [0,1]$. Notice that the first level consists of four squares with sides equal to $\frac{1}{2}$, Γ_2 contains 4^2 squares with sides equal to $\frac{1}{2^2}$, and in general, level n consists of 4^n squares with sides equal to $\frac{1}{2^n}$.

In particular, if there exists $\dim_B(F)$*, then we have*

$$\dim_B(F) = 2 \cdot \lim_{\delta \to 0} \frac{\log \mathcal{N}_\delta(\alpha^{-1}(F))}{-\log \delta}. \tag{1}$$

To deal with the construction of the curve α, we refer the reader to [4, Section 2.4]. For more information on this mathematica invariant see [3].

3. Results and discussion

3.1. Description of the sample

In this section, we shall describe the sample of patients that took part in our study. 77 subjects were involved with 80.5% (62 people) being women. Each patient was assigned to one of the three following groups. Group 1 consists of 60 patients, all of them without loss of teeth, 10 subjects were assigned to group 2 (with the absence of some dental pieces), and group 3 consists of 7 total edentulous patients. A first descriptive analysis was carried out with the aim to characterise our sample of patients. As such, for each patient in our study, the following attributes were considered.

1. **Age**: it was found a mean age equal to 53.2 years with a standard deviation of 9 years.
2. **DCV**: a mean of 7.74 and a standard deviation equal to 2 (a variance of 2.7) were found.
3. **DCP**: with a mean of 3.93 and a standard deviation equal to 2 (a variance of 2.6).
4. **DVD**: a mean of 12.9 and a standard deviation of 2 (a variance equal to 2.6) were obtained.
5. **DVI**: with a mean of 12.8 and a standard deviation equal to 2 (a variance equal to 2.3).
6. **Area**: they were found a mean of 5.32 and a standard deviation equal to 2 (a variance of 5.0).
7. **W**: a mean equal to 2.94 and a standard deviation of 0.7 (a variance of 0.48) were found.
8. **H**: with a mean equal to 2.23 and a standard deviation of 0.6 (a variance of 0.31).
9. **Mean**: they were obtained a mean equal to 170.067 and a standard deviation of 116.598 (a variance of 13595.1).
10. **DIM**: a mean fractal dimension of 1.68 and a standard deviation equal to 0.08 (a variance of 0.0069) were found.

Table 1 summarizes the sample description by attributes.

3.2. Sample description by sex

Next, we shall describe in detail our sample of patients by sex groups.

	Whole sample ($n = 77$)			Male Group ($n = 15$)			Female Group ($n = 62$)		
Attribute	**Mean**	**Std. dev.**	**Variance**	**Mean**	**Std. dev.**	**Variance**	**Mean**	**Std. dev.**	**Variance**
Age	53.2	9		55.1	7		52.7	9	
DCV	7.74	2	2.7	8.83	1	2.1	7.48	2	2.5
DCP	3.93	2	2.6	4.21	1	1.9	3.87	2	2.9
DVD	12.9	2	2.6	13.4	2	3.2	12.8	2	2.5
DVI	12.8	2	2.3	13.5	2	2.3	12.7	1	2.1
Area	5.32	2	5.0	5.1	2	6.1	5.37	2	4.8
W	2.94	0.7	0.48	2.88	0.7	0.44	2.96	0.7	0.5
H	2.23	0.6	0.31	2.21	0.7	0.53	2.24	0.5	0.26
MEAN	170.067	116.598	13595.1	190.415	99.5001	9900.27	165.144	120.58	14539.5
DIM	1.68	0.08	0.0069	1.7	0.08	0.0072	1.67	0.08	0.0068

Table 1. Sample description by attributes.

3.2.1. Female population

It contains 62 subjects (80.5% of the whole sample) of which 50 people were assigned to group 1, 8 to group 2, and 4 to group 3. In regard to the attributes explored for each female patient in the present study, the results we obtained are as follows.

1. **Age**: a mean age of 52.7 years with a standard deviation equal to 9 years was found.
2. **DCV**: a mean equal to 7.48 and a standard deviation of 2 (a variance of 2.5) were obtained.
3. **DCP**: with a mean equal to 3.87 and a standard deviation equal to 2 (a variance of 2.9).
4. **DVD**: they were found a mean of 12.8 and a standard deviation equal to 2 (a variance of 2.5).
5. **DVI**: it was found a mean equal to 12.7 with a standard deviation of 1 (a variance equal to 2.1).
6. **Area**: with a mean equal to 5.37 and a standard deviation equal to 2 (a variance of 4.8).
7. **W**: a mean equal to 2.96 and a standard deviation of 0.7 (a variance of 0.5) were found.
8. **H**: they were found a mean of 2.24 and a standard deviation equal to 0.5 (a variance of 0.26).
9. **Mean**: a mean of 165.144 and a standard deviation of 120.58 (a variance equal to 14539.5) were obtained.
10. **DIM**: a mean fractal dimension of 1.67 and a standard deviation equal to 0.08 (a variance of 0.0068) were found.

3.2.2. Male population

15 people (19.5% of the whole sample) in our study are men. Of them, 10 were assigned to group 1, 2 to group 2, and 3 to group 3. Similarly to our female population, some descriptive statistics regarding the attributes of the male one were calculated. The results are provided below.

1. **Age**: it was found a mean age equal to 55.1 years with a standard deviation of 7 years.
2. **DCV**: a mean of 8.83 and a standard deviation equal to 1 (a variance of 2.1) were found.
3. **DCP**: with a mean of 4.21 and a standard deviation equal to 1 (a variance of 1.9).
4. **DVD**: a mean of 13.4 and a standard deviation of 2 (a variance equal to 3.5) were obtained.
5. **DVI**: with a mean equal to 13.4 and a standard deviation of 2 (a variance equal to 3.2).
6. **Area**: they were found a mean of 5.1 and a standard deviation equal to 2 (a variance of 6.1).
7. **W**: a mean equal to 2.88 and a standard deviation of 0.7 (a variance of 0.44) were found.
8. **H**: with a mean of 2.21 and a standard deviation equal to 0.7 (a variance of 0.53).
9. **Mean**: they were obtained a mean equal to 190.415 and a standard deviation of 99.5001 (a variance of 9900.27).
10. **DIM**: a mean fractal dimension equal to 1.7 and a standard deviation of 0.08 (a variance of 0.0072) were found.

3.3. Some comparisons by sex

Some preliminary comparisons were carried out between each attribute for both the female and the male populations involved in this study. The obtained results appear below. All the conclusions were obtained by working at a confidence level of 95%.

1. **Age**: no significative differences were found. In fact, a p-value equal to 0.260007 was obtained by Mann-Whitney test (a p-value of 0.463741 was provided by Student's t-test).
2. **DCV**: in this case, significative differences were found by a p-value of 0.00334195*[1] in Mann-Whitney test (a p-value equal to 0.00538115* by Student's t-test).
3. **DCP**: they were found no significative differences by a Mann-Whitney p-value equal to 0.30891.
4. **DVD**: a p-value of 0.245115 was provided by Mann-Whitney test (resp., a p-value equal to 0.26562 was thrown by Student's t-test). As such, they were found no significative differences.
5. **DVI**: Mann-Whitney test provided a p-value equal to 0.117541 (resp., a p-value of 0.0706976 was obtained by Student's t-test). Thus, no significative differences were found.
6. **Area**: no differences were observed. In fact, Mann-Whitney test provided a p-value equal to 0.459336.
7. **W**: A p-value of 0.968215 in Mann-Whitney test (resp., a p-value equal to 0.939092 in Student's t-test) was found. As such, they were found no significative differences.
8. **H**: They were no significative differences. In fact, Mann-Whitney test provided a p-value of 0.298489.
9. **Mean**: Mann-Whitney test threw a p-value equal to 0.447607 (resp., a p-value of 0.598811 was found by Student's t-test), so they were found no significative differences.
10. **DIM**: no significative differences were found. In fact, a p-value of 0.371378 was provided by Mann-Whitney test (resp, a p-value equal to 0.314657 in Student's t-test).

3.4. A first step towards symmetry

We compared the variable DVD (distance right side wall nasoplatine hole to right canine mamelon) to DVI (distance left lateral wall nasoplatine hole to left canine mamelon) regarding the female population. As a result, they were found no significant differences at a significance level of 95%. In fact, we obtained a p-value equal to 0.765075 in Mann-Whitney test (resp., a p-value of 0.854011 by Student's t-test). Thus, both variables DVD and DVI behave symmetrically in regard to the female population. A similar study was carried out concerning the male population. A p-value equal to 0.603301 in Mann-Whitney test (resp., a p-value of 0.594769 by Student's t-test) also highlights a symmetric behavior between these two lateral variables.

3.5. Fractal dimension analysis

The fractal dimensions of 77 binary images from each patient in our sample have been accurately calculated and analysed. To deal with, an appropriate collection of scanners was selected from each patient taking part in our study. Next step was to convert such scanners to binary images by assigning "ones" to those pixels exceeding a certain color threshold and "zeros" otherwise. For illustration purposes, Fig. 3 provides a graphical representation of an actual scanner from a subject that took part in our study and its binary images.

Thus, a mean fractal dimension equal to 1.68 and a standard deviation of 0.08 (a variance equal to 0.0069) were found. We also extracted both left and right sides of each binary image in the sample and calculated their fractal dimensions. A mean fractal dimension equal to 1.68 and a standard deviation of 0.1 (a variance equal to 0.015) were obtained for the left side binary images. Similarly, a mean fractal dimension of 1.68 and a standard deviation equal to 0.1 (a variance of 0.011) were found for the right side images. The results of the fractal dimension analysis carried out for each kind of binary images

[1] * means that significative differences were found at a confidence level of 95%.

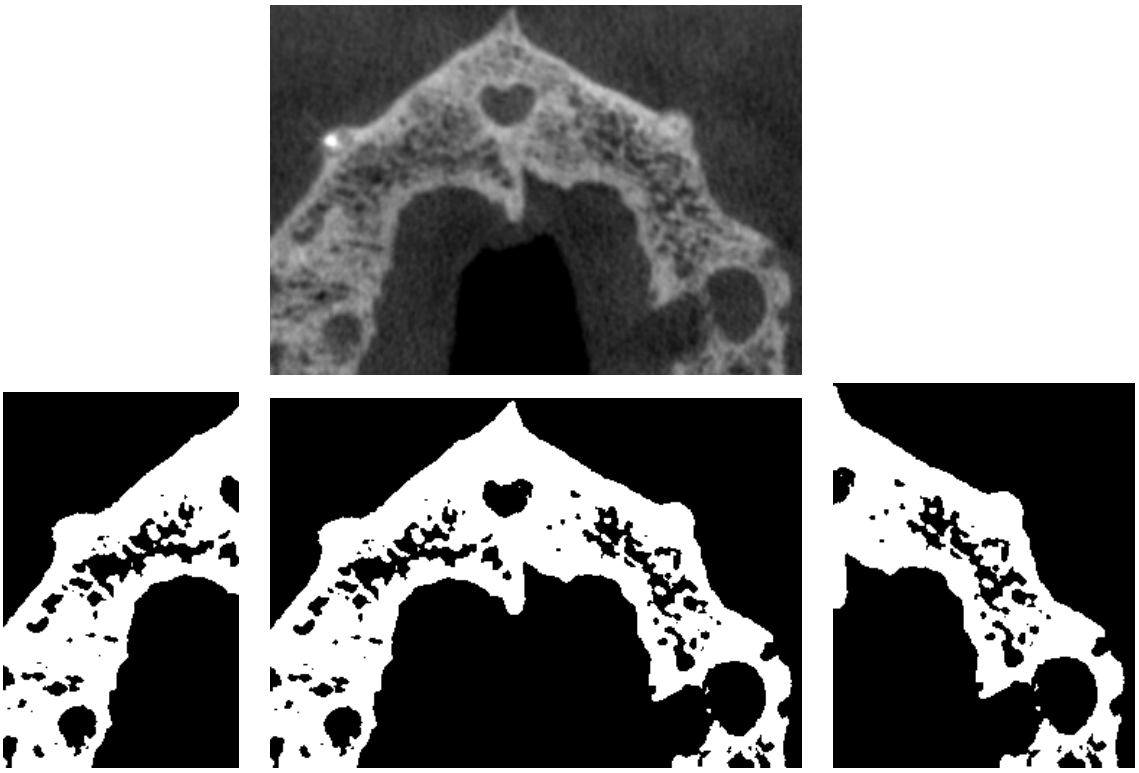

Figure 3. Graphical representation of an actual scanner from a patient that took part in our study (left) and its corresponding binary images.

		Dim. of binary images			Dim. of Left images			Dim. of Right images		
	n	**Mean**	**Std. dev.**	**Variance**	**Mean**	**Std. dev.**	**Variance**	**Mean**	**Std. dev.**	**Variance**
Whole sample	77	1.68	0.08	0.0061	1.69	0.1	0.013	1.68	0.1	0.0097
Group 1	60	1.68	0.07	0.0052	1.68	0.09	0.0085	1.68	0.09	0.0078
Group 2	10	1.65	0.1	0.016	1.6	0.2	0.046	1.66	0.1	0.016
Group 3	7	1.69	0.1	0.011	1.73	0.2	0.03	1.71	0.2	0.033

Table 2. Results of the fractal dimension analysis for each kind of binary images and each group.

and each group appear in Table 2. The differences (in absolute value) between the fractal dimensions from each left binary image and its corresponding right side one were calculated. Thus, a mean difference equal to 0.07 with a standard deviation of 0.06 (a variance equal to 0.003) were obtained. Table 3 contains the results of the analysis of the differences among the fractal dimensions of each left binary image and its corresponding right side one for each group. In addition, Fig. (4) (left, first row) illustrates the empirical distribution of the fractal dimension values for all the 77 binary images analysed as well as the empirical distribution of the fractal dimensions from their corresponding lateral binary images. In addition, the empirical distribution of the differences between each left binary image and its corresponding right side one is depicted in Fig. (4) (right, first row).

At a confidence level of 95%, a p-value equal to 0.893639 (resp., a p-value of 0.921788) was found by Mann-Whitney test (resp., by Student's t-test) when comparing the fractal dimension values of the left side binary images with respect to the fractal dimensions of their corresponding right side ones for all the subjects in the sample. That empirical result suggests a symmetric behavior of the fractal dimension of both lateral binary images from each patient involved in the present study.

Next, we analyse in detail the fractal dimension of the binary images of the subjects from each of the three groups they were assigned to.

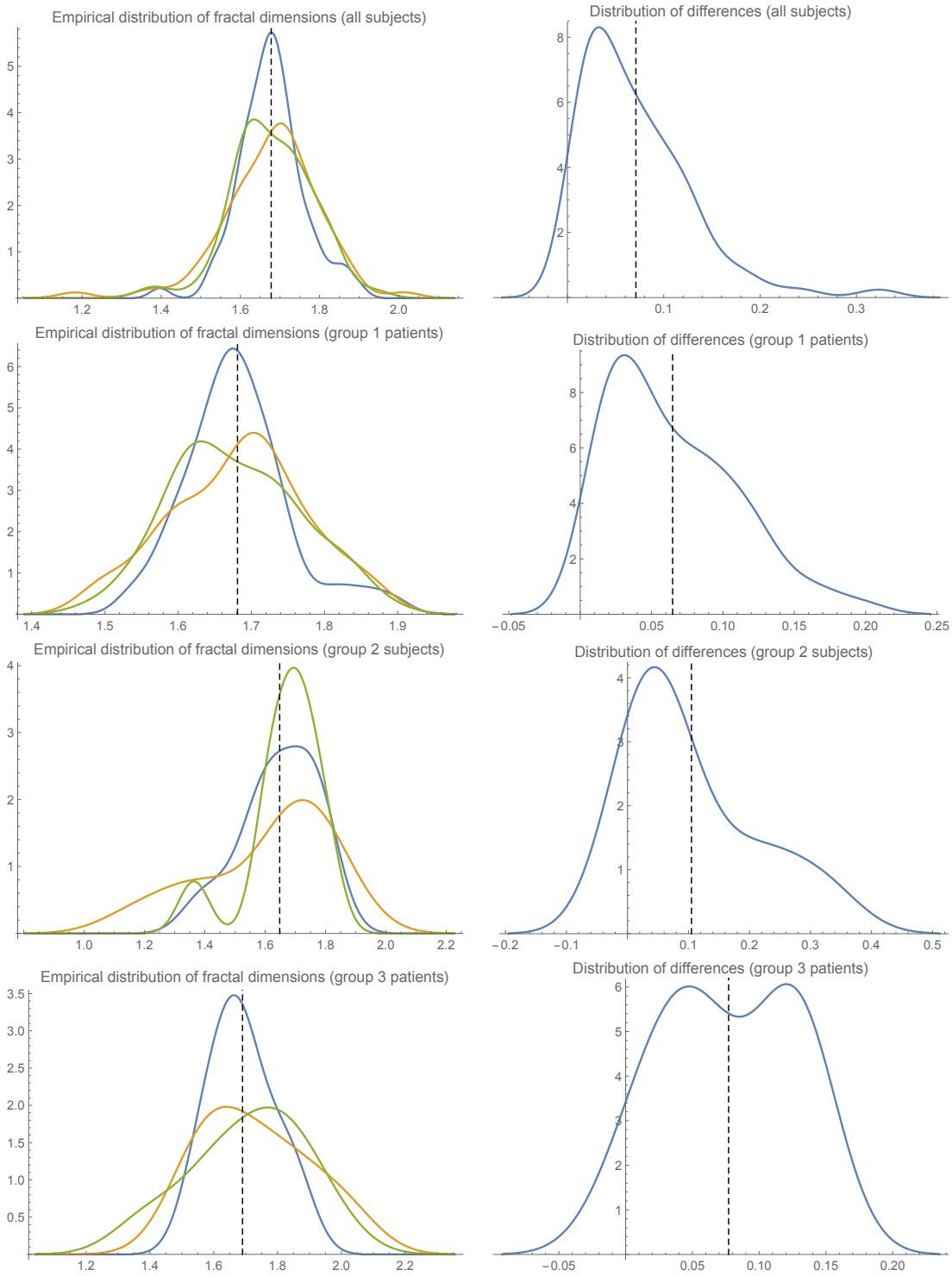

Figure 4. The blue line in each plot at the left illustrates the empirical distribution of the fractal dimension values for all the binary images analysed from each group in our patient sample. Further, the discontinuous line marks the mean fractal dimension of the binary images from all the scanners analysed. Notice also that the orange line (resp., the green line) represents the empirical distribution of the fractal dimensions of the left side (resp., the right side) binary images from each group of patients. On the other hand, each graph at the right depicts the empirical distribution of the differences (in absolute value) between each left side binary image and its corresponding right side one from each group of patients. The discontinuous line represents the mean of such differences.

	Differences (in abs.) among Left and Right fractal dimensions				
	Mean	**Std. dev.**	**Variance**	**Mann-Whitney**	**Student's t-test**
Whole sample	0.07	0.06	0.004	0.703184	0.738849
Group 1	0.06	0.05	0.002	0.727063	0.775088
Group 2	0.1	0.1	0.01	0.73373	0.455717
Group 3	0.08	0.05	0.003	0.898327	0.794665

Table 3. Analysis of the differences among the fractal dimensions of each left binary image and its corresponding right side one for each group.

3.6. Fractal dimension analysis for group 1 patients

Group 1 contains 60 subjects. A mean fractal dimension of 1.68 with a standard deviation equal to 0.07 (a variance of 0.0052) was found. Moreover, we obtained a mean fractal dimension equal to 1.68 and a standard deviation of 0.09 (a variance equal to 0.0085) regarding the left side binary images for all the patients assigned to group 1. Similarly, they were obtained a mean fractal dimension of 1.68 and a standard deviation equal to 0.09 (a variance of 0.0078) for the right side images from the subjects in group 1. Further, for each patient in group 1, they were analysed the differences (in absolute value) between the fractal dimension of each right side image and the fractal dimension of its corresponding left side one. As such, a mean difference equal to 0.06 and a standard deviation of 0.05 (a variance equal to 0.002) were found. Similarly to Fig. (**??**), Fig. (4) (left, second row) shows the empirical distribution of the fractal dimensions of all the 60 binary images of each subject in group 1 as well as the empirical distribution of the fractal dimensions of their corresponding lateral images. On the other hand, Fig. (4) (right, second row) illustrates the empirical distribution of the differences between the fractal dimension of each left side image and the fractal dimension of its corresponding right side one for the subjects in group 1. A p-value equal to 0.727063 (resp., a p-value of 0.775088) was provided by Mann-Whitney test (resp., by Student's t-test) when comparing the fractal dimension values of the left side binary images with respect to the fractal dimensions of their corresponding right side ones for all the subjects in group 1 (at a confidence level of 95%). That empirical result suggests a symmetric behavior of the fractal dimension of both lateral binary images from each patient assigned to group 1.

3.7. Fractal dimension analysis for patients in group 2

Group 2 consists of 10 subjects. A mean fractal dimension of 1.65 with a standard deviation equal to 0.1 (a variance of 0.016) was found. Moreover, we obtained a mean fractal dimension equal to 1.6 and a standard deviation of 0.2 (a variance equal to 0.046) regarding the left side binary images for all the patients assigned to group 1. Similarly, they were obtained a mean fractal dimension of 1.66 and a standard deviation equal to 0.1 (a variance of 0.016) for the right side images from the subjects in group 1. Further, for each patient in group 2, they were analysed the differences (in absolute value) between the fractal dimension of each right side image and the fractal dimension of its corresponding left side one. As such, a mean difference equal to 0.1 and a standard deviation of 0.1 (a variance equal to 0.01) were found. Fig. (4) (left, third row) shows the empirical distribution of the fractal dimensions of all the 10 binary images of each subject in group 2 as well as the empirical distribution of the fractal dimensions of their corresponding lateral images. On the other hand, Fig. (4) (right, third row) illustrates the empirical distribution of the differences between the fractal dimension of each left side image and the fractal dimension of its corresponding right side one for the subjects in group 2.

A p-value equal to 0.73373 (resp., a p-value of 0.455717) was provided by Mann-Whitney test (resp., by Student's t-test) when comparing the fractal dimension values of the left side binary images with respect to the fractal dimensions of their corresponding right side ones for all the subjects in group 2 (at a confidence level of 95%). That empirical result highlights a symmetric behavior of the fractal dimension of both lateral binary images from each patient assigned to group 2.

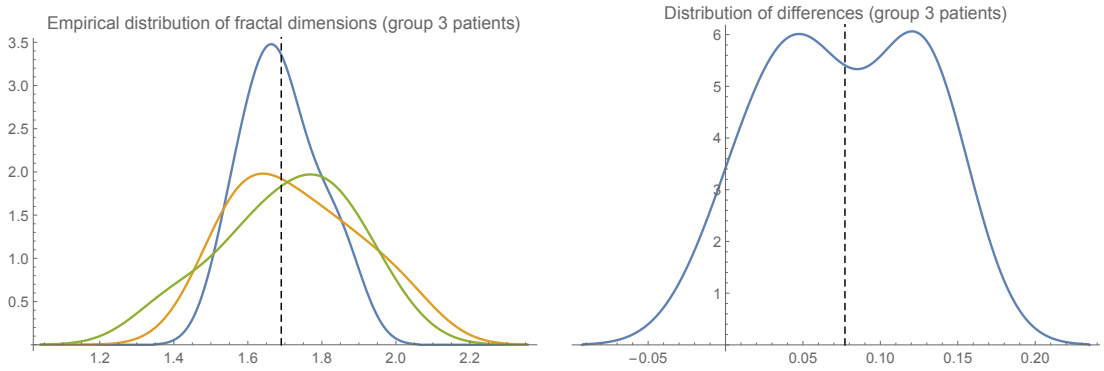

Figure 5. The blue line in the plot at the left illustrates the empirical distribution of the fractal dimension values for the 7 binary images of the subjects in group 3. Notice that the orange line (resp., the green line) represents the empirical distribution of the fractal dimension for all the left side (resp., the right side) binary images from each patient scanner. Moreover, the discontinuous line marks the mean fractal dimension of the binary images from all the scanners of group 3 that were analysed. On the other hand, the graph at the right shows the empirical distribution of the differences (in absolute value) between each left side binary image and its corresponding right side one for each patient assigned to group 3. The discontinuous line represents the mean of such differences.

3.8. Fractal dimension analysis for patients in group 3

7 subjects were assigned to group 3. A mean fractal dimension of 1.69 with a standard deviation equal to 0.1 (a variance of 0.011) was found. Moreover, we obtained a mean fractal dimension equal to 1.73 and a standard deviation of 0.2 (a variance equal to 0.03) regarding the left side binary images for all the patients assigned to group 3. Also, they were obtained a mean fractal dimension of 1.71 and a standard deviation equal to 0.2 (a variance of 0.033) for the right side images from the subjects in group 3. In addition, for each patient in that group, they were analysed the differences (in absolute value) between the fractal dimension of each right side image and the fractal dimension of its corresponding left side one. Thus, a mean difference equal to 0.08 and a standard deviation of 0.05 (a variance equal to 0.003) were found. Fig. (4) (left, fourth row) shows the empirical distribution of the fractal dimensions of all the 7 binary images of each subject in group 3 as well as the empirical distribution of the fractal dimensions of their corresponding lateral images. On the other hand, Fig. (4) (right, fourth row) depicts the empirical distribution of the differences between the fractal dimension of each left side image and the fractal dimension of its corresponding right side one for the subjects in group 3.

A p-value equal to 0.898327 (resp., a p-value of 0.794665) was provided by Mann-Whitney test (resp., by Student's t-test) when comparing the fractal dimension values of the left side binary images with respect to the fractal dimensions of their corresponding right side ones for all the subjects in group 3 (at a confidence level of 95%). That empirical result shows a symmetric behavior of the fractal dimension of both lateral binary images from each patient assigned to group 3.

3.9. Analysis of fractal dimension by groups

In this section, we shall perform a pairwise comparison by groups in regard to the fractal dimensions of the binary images that were assigned to each of them.

3.9.1. Fractal dimension comparison between groups 1 and 2

Firstly, we compared the medians (resp., the means) of the fractal dimensions of the binary images assigned to each of the groups 1 and 2 at a confidence level of 95%. In this way, no significative differences were found. In fact, a p-value equal to 0.608721 (resp., a p-value of 0.445315) was

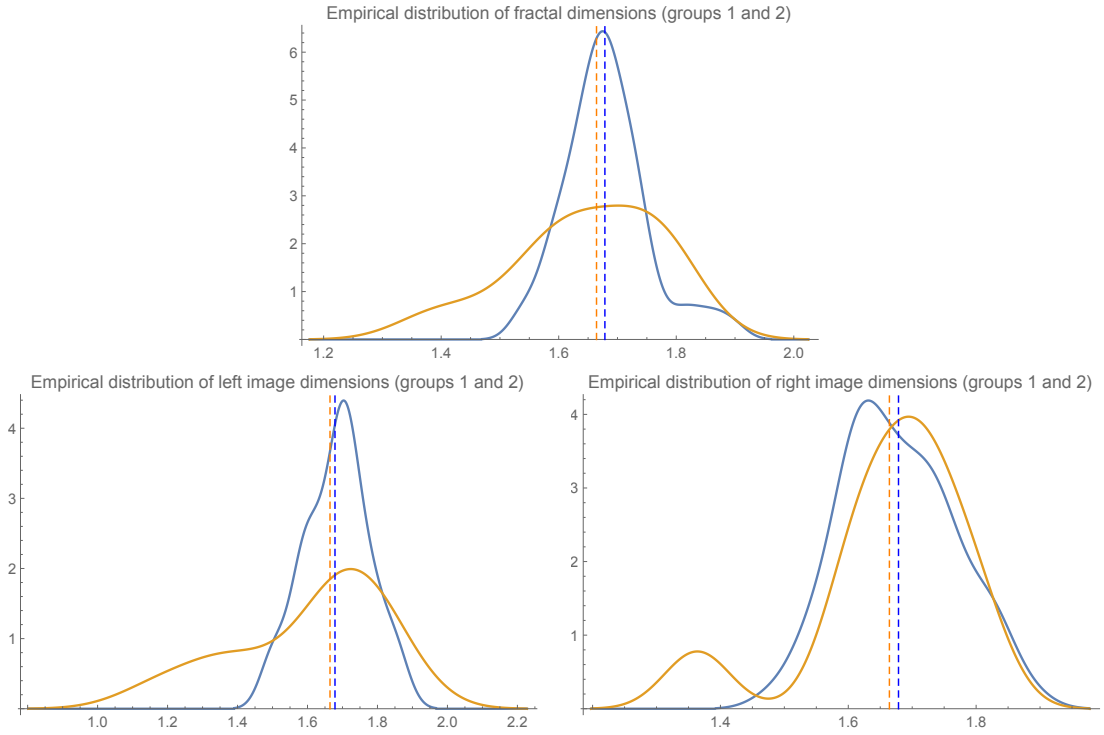

Figure 6. Empirical distributions of the fractal dimensions of the binary images from both groups 1 (blue line) and 2 (picture at the first row) and empirical distributions of the fractal dimensions of their lateral binary images (second row). The discontinuous straight lines mark the mean fractal dimension of each group and each kind of binary images.

	Dim. comparison by groups: 1 vs. 2		
	Whole images	**Left images**	**Right images**
Mann-Whitney	0.608721	0.597025	0.939796
Student's t-test	0.445315	0.284107	0.663177

Table 4. Statistical comparison of medians (resp., means) of the fractal dimensions of each kind of image and group. They are provided by p-values from Mann-Whitney test (resp., from Student's t-test) involving groups 1 and 2. No significative differences were found at a confidence level of 95%.

provided by Mann-Whitney test (resp., by Student's t-test). Fig. (6) (first row) compares the empirical distributions of the fractal dimensions of all the binary images in each group.

The medians (resp., means) of the fractal dimensions of the left binary images from each of the groups 1 and 2 were compared. Fig. (6) (second row, left) depicts the empirical distributions of the fractal dimensions of the left binary images in each group. A p-value of 0.597025 (resp., a p-value equal to 0.284107) was found by Mann-Whitney test (resp., by Student's t-test) at a confidence level of 95%. That result throws some empirical evidence regarding a similar behavior of the empirical distributions of the fractal dimensions of the left binary images from both groups. The fractal dimensions of the right side images from groups 1 and 2 were compared similarly. Fig. (6) (second row, right) illustrates the empirical distributions of the fractal dimensions of the right binary images in each group. A p-value of 0.939796 (resp., a p-value equal to 0.663177) was found by Mann-Whitney test (resp., by Student's t-test) at a confidence level of 95%. Table 4 summarizes the results of the statistical comparison of medians (resp., means) of the fractal dimensions of each kind of image and group. They suggest that the empirical distributions of the fractal dimensions of the right binary images from both groups are similar.

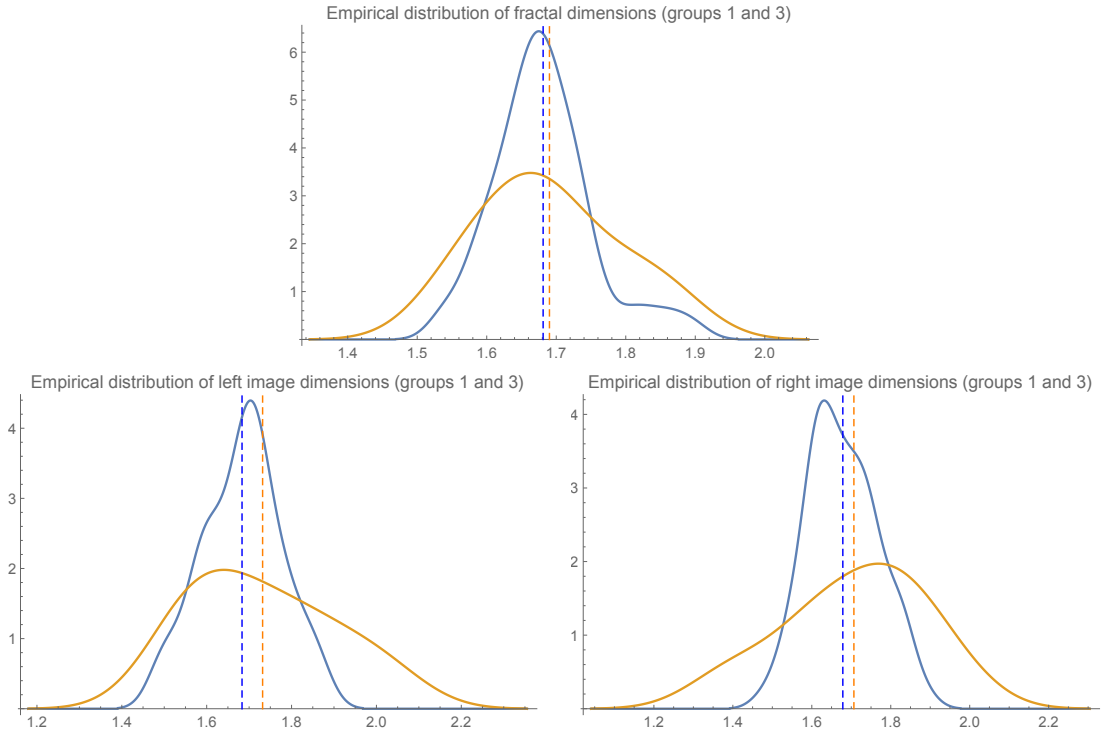

Figure 7. Empirical distributions of the fractal dimensions of the binary images from both groups 1 (blue line) and 3 (picture at the first row) and empirical distributions of the fractal dimensions of their lateral binary images (second row). The discontinuous straight lines mark the mean fractal dimension of each group and each kind of binary images.

3.9.2. Fractal dimension comparison between groups 1 and 3

The medians (resp., the means) of the fractal dimensions of the binary images from each of the groups 1 and 3 were compared. No significative differences were found at a confidence level of 95%. In fact, a p-value equal to 0.829589 (resp., a p-value of 0.772554) was provided by Mann-Whitney test (resp., by Student's t-test). Fig. (7) (first row) compares the empirical distributions of the fractal dimensions of all the binary images in each group.

The medians (resp., means) of the fractal dimensions of the left binary images from each of the groups 1 and 3 were also compared. Fig. (7) (second row, left) depicts the empirical distributions of the fractal dimensions of the left binary images in each group. A p-value of 0.55909 (resp., a p-value equal to 0.488576) was found by Mann-Whitney test (resp., by Student's t-test) at a confidence level of 95%. That result throws some empirical evidence regarding a similar behavior of the empirical distributions of the fractal dimensions of the left binary images from both groups. The fractal dimensions of the right side images from groups 1 and 3 were compared similarly. Fig. (7) (second row, right) illustrates the empirical distributions of the fractal dimensions of the right binary images in each group. A p-value of 0.46681 (resp., a p-value equal to 0.687664) was found by Mann-Whitney test (resp., by Student's t-test) at a confidence level of 95%. Table 5 contains the results of the statistical comparison of medians (resp., means) of the fractal dimensions of each kind of image and group. They suggest that the empirical distributions of the fractal dimensions of the right binary images from both groups are similar.

3.9.3. Fractal dimension comparison between groups 2 and 3

The medians (resp., the means) of the fractal dimensions of the binary images from each of the groups 2 and 3 were also compared. Once again, no significative differences were found at a confidence level of 95%. In fact, a p-value equal to 0.660549 (resp., a p-value of 0.487739) was

	Dim. comparison by groups: 1 vs. 3		
	Whole images	**Left images**	**Right images**
Mann-Whitney	0.829589	0.55909	0.46681
Student's t-test	0.772554	0.488576	0.687664

Table 5. Statistical comparison of medians (resp., means) of the fractal dimensions of each kind of image and group. They are provided by p-values from Mann-Whitney test (resp., from Student's t-test) involving groups 1 and 3. No significative differences were found at a confidence level of 95%.

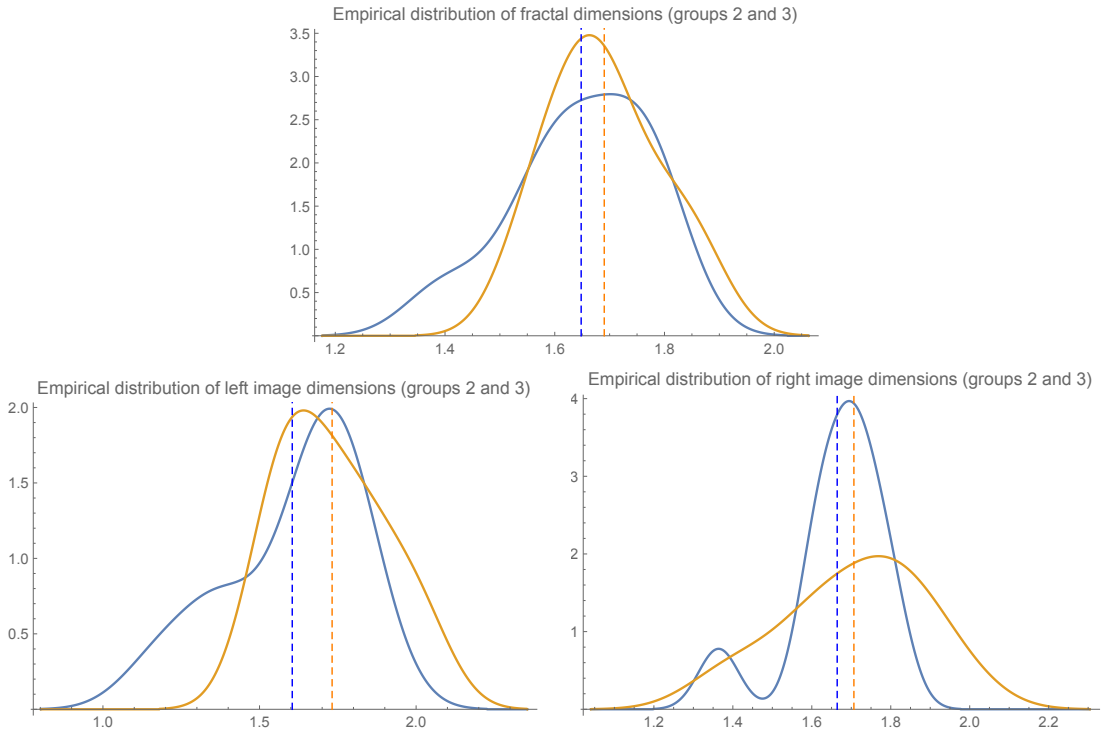

Figure 8. Empirical distributions of the fractal dimensions of the binary images from both groups 2 (blue line) and 3 (picture at the first row) and empirical distributions of the fractal dimensions of their lateral binary images (second row). The discontinuous straight lines mark the mean fractal dimension of each group and each kind of binary images.

provided by Mann-Whitney test (resp., by Student's t-test). Fig. (8) (first row) compares the empirical distributions of the fractal dimensions of all the binary images in each group.

The medians (resp., means) of the fractal dimensions of the left binary images from each of the groups 2 and 3 were compared as well. Fig. (8) (second row, left) depicts the empirical distributions of the fractal dimensions of the left binary images in each group. A p-value of 0.406813 (resp., a p-value equal to 0.214816) was found by Mann-Whitney test (resp., by Student's t-test) at a confidence level of 95%. That result provides some empirical evidence regarding a similar behavior of the empirical distributions of the fractal dimensions of the left binary images from both groups. The fractal dimensions of the right side images from groups 2 and 3 were compared similarly. Fig. (8) (second row, right) illustrates the empirical distributions of the fractal dimensions of the right binary images in each group. A p-value of 0.464214 (resp., a p-value equal to 0.566228) was found by Mann-Whitney test (resp., by Student's t-test) at a confidence level of 95%. Table 6 collects the results of the statistical comparison of medians (resp., means) of the fractal dimensions of each kind of image and group. They throw some empirical evidence in regard to a similar behavior of the empirical distributions of the fractal dimensions of the right binary images from both groups.

	Dim. comparison by groups: 2 vs. 3		
	Whole images	**Left images**	**Right images**
Mann-Whitney	0.660549	0.406813	0.464214
Student's t-test	0.487739	0.214816	0.566228

Table 6. Statistical comparison of medians (resp., means) of the fractal dimensions of each kind of image and group. They are provided by p-values from Mann-Whitney test (resp., from Student's t-test) involving groups 1 and 3. No significative differences were found at a confidence level of 95%.

4. Conclusions

All the anatomical considerations that surround the nasopalalatin foramen have been described along this paper. Regarding them, an analysis of bone density via an efficient calculation of fractal dimension has been carried out in that area. A sample with 77 patients was considered. 60 of them were assigned to group 1 (without loss of teeth), 10 to group 2 (with the absence of some teeth), and 7 to group 3 (with all its subjects being total edentulous). 63 women took part in the final stage of our study. The mean age of the patients was equal to 53.2 years with a standard deviation of 9 years. For each subject, cone beam computed tomography was performed for treatment needs. A specific window, which coincides with an axial cut at the level of the anterior nasal spine, was selected. In that area, different anthropometric measurements were performed. In addition, we applied a novel and accurate approach to calculate the fractal dimension of binary images generated from each patient CBCT scanner. Three types of binary images were used for each subject including both right and left sides from the original one. Mann-Whitney test and Student's t-test threw some statistical evidence regarding a symmetric behavior of such binary images. Moreover, we found no significative differences regarding the anthropometric measures explored in the different groups of our study. Accordingly, several patterns of symmetry were appreciated at a whole range of levels.

Author Contributions: All authors of this paper have contributed in an equal way to the results presented.

Funding: This paper has been partially supported by grant No. MTM2015-64373-P (MINECO/FEDER, UE), MINECO grant number MTM2014-51891-P and Fundación Séneca de la Región de Murcia grant number 19219/PI/14.

Conflicts of Interest: Declare conflicts of interest or state "The authors declare no conflict of interest.".

References

1. Bornstein M. M., Balsiger R., Sendi P., and von Arx T., Morphology of the nasoplatine canal and dental implant surgery: a radiographic analysis of 100 consecutive patients using limited cone beam computed tomography. *Clinical Oral Implants Research* **2011**, *22 (3)*, 295-301, doi:10.1111/j.1600-0501.2010.02010.x
2. Chimenos Kustner E., Ribera Uribe M., López López J., Gerodontología; Sociedad Española de Gerodontología: Santiago de Compostela, Spain, 2012; ISBN: 978-84-695-3382-6
3. Fernández-Martínez, M., A survey on fractal dimension for fractal structures. *Applied Mathematics and Nonlinear Sciences*, **2016**, *1 (2)*, 437-472.
4. Fernández-Martínez, M., Gómez García, F. J., Sánchez Guerrero, Y., and López Jornet, Pía, An intelligent system to study the fractal dimension of trabecular bones. *Journal of Intelligent & Fuzzy Systems*, **2018**, *35 (4)*, 4533-4540, doi:10.3233/JIFS-169772
5. Gómez de Ferraris M. E. and Campos Muñoz A, Histología, Embriología e Ingeniería Tisular Bucodental; Panamericana, Madrid, 2009; ISBN: 978-607-7743-01-9
6. Hakbilen S. and Magat G., Evaluation of anatomical and morphological characteristics of the nasoplatine canal in a Turkish population by cone beam computed tomography. *Folia Morphologica* **2018**, *77 (3)*, 527-535, doi:10.5603/FM.a2018.0013
7. Jolley, L., Majumdar, S., and Kapila, S., Technical factors in fractal analysis of periapical radiographs. *Dentomaxillofacial Radiology*, **2006**, *35 (6)*, 393-397, doi:10.1259/dmfr/30969642

8. Liang X., Jacobs R., Martens W., Hu YQ., Adriaensens P., Quirynen M., and Lambrichts I., Macro- and micro-anatomical, histological and computed tomography scan characterization of the nasoplatine canal. *Journal of Clinical Periodontology* **2009**, *36 (7)*, 598-603, doi:10.1111/j.1600-051X.2009.01429.x
9. López Muñiz A., Hernández González L.C., del Valle Soto M., Suárez Garnacho S., Carbajo Pérez E., and Junceda Moreno J., Anatomía Topográfica Humana; Ediciones de la Universidad de Oviedo: Oviedo, Spain, 2008; ISBN: 978-84-7468-911-2
10. Misch, C. E., Contemporary Implant Dentistry; Mosby Elsevier: St. Louis, Missouri, USA, 2008; ISBN: 978-0-323-04373-1
11. Nart Molina J., Marcuschamer Gittler E., Rumeu Milá J., Santos Alemany A., and Griffin T.J., Preservación del reborde alveolar. Por qué y cuándo. *Periodoncia y Osteointegración* **2007**, *17 (4)*, 229-237, doi:
12. Shah N., Bansal N., and Logani A., Recent advances in imaging technologies in dentistry. *World Journal of Radiology* **2014**, *6 (10)*, 794-807, doi:10.4329/wjr.v6.i10.794
13. Ruttimann U. E., Webber R. L., and Hazelrig J. B., Fractal dimension from radiographs of peridental alveolar bone. *Oral Surgery, Oral Medicine, Oral Pathology* **1992**, *74 (1)*, 98-110, doi:10.1016/0030-4220(92)90222-C
14. Sindeaux R., de Souza Figueiredo P. T., Santos de Melo Nilce, Bittencourt Guimarães A. T., Lazarte L., Borges Pereira F., de Paula A. P., and Ferreira Leite A., Fractal dimension and mandibular cortical width in normal and osteoporotic men and women. *Maturitas*, **2014**, *77 (2)*, 142-148, doi:10.1016/j.maturitas.2013.10.011
15. Velayos Santana J.L., Anatomía de la cabeza para odontólogos; Panamericana, Madrid, 2007; ISBN: 978-84-9835-068-5

Sample Availability: Samples of the compounds ..... are available from the authors.